LAWRENCE
LIVERMORE
NATIONAL
LABORATORY

Titanium and germanium lined hohlraums and halfraums as multi-keV X-ray radiators

F. Girard, M. Primout, K. B. Fournier, B. Villette, P. Stemmler, L. Jacquet, D. Babonneau

May 28, 2009

Disclaimer

This document was prepared as an account of work sponsored by an agency of the United States government. Neither the United States government nor Lawrence Livermore National Security, LLC, nor any of their employees makes any warranty, expressed or implied, or assumes any legal liability or responsibility for the accuracy, completeness, or usefulness of any information, apparatus, product, or process disclosed, or represents that its use would not infringe privately owned rights. Reference herein to any specific commercial product, process, or service by trade name, trademark, manufacturer, or otherwise does not necessarily constitute or imply its endorsement, recommendation, or favoring by the United States government or Lawrence Livermore National Security, LLC. The views and opinions of authors expressed herein do not necessarily state or reflect those of the United States government or Lawrence Livermore National Security, LLC, and shall not be used for advertising or product endorsement purposes.

Titanium and germanium lined hohlraums and halfraums as multi-keV X-ray radiators.

F. Girard[1], M. Primout[1], K.B. Fournier[2], B. Villette[1], Ph. Stemmler[1], L. Jacquet[1] and D. Babonneau[1]

[1] CEA DAM DIF, F-91297 Arpajon, France
[2] LLNL, P.O. Box 808, Livermore, California 94550, USA

As multi-keV x-ray radiators, hohlraums and halfraums with inner walls coated with metallic materials (called liner) have been tested for the first time with a laser as the energy drive. For titanium, conversion efficiencies (CEs) are up to ~14% for emission into 4π, integrating between 4.6 and 6.5 keV when a large diameter hohlraum is used. Germanium CE is ~0.8% into 4π between 9 and 13 keV. The highest conversion efficiencies have been obtained with a 1ns squared pulse and phase plates giving laser absorption near 99%. These high CEs are due to long-lasting, good plasma conditions for multi-keV x-ray production maintained by plasma confinement inside the plastic cylinder and plasma collision leading to a burst of x rays at a time that depends on target size. As photon emitters at 4.7 keV, titanium-lined hohlraums are the most efficient solid targets and data are close to CEs for gas targets, which are considered as the upper limit for x-ray yields since their low density allow good laser absorption and low kinetics losses. As 10.3 keV x-ray emitters, exploded germanium foils give best results one order of magnitude more efficient than thick targets; doped aerogels and lined hohlraums give similar yields, about 3 times lower than those from exploded foils.

I. INTRODUCTION

X-ray sources in the range of 5–50 keV are required for diagnostics of inertial confinement fusion experiments, as backlighting sources for dense matter probing and material testing [1–3]. Multi-keV x-ray sources from laser-heated plasmas have been investigated by laser irradiation of solid targets [4–9]. Solid targets enable the creation of multi-keV sources at various photon energies but exhibit low laser-to-x-ray conversion efficiencies. Underdense radiators such as gas and doped-aerogel targets are more efficient multi-keV x-ray converters since hydrodynamic losses are lower, heating is faster and the laser-absorption volume is wider but they have a spectral domain limited to photon energies accessible with materials for which such targets can be made [10,11]. Underdense target experiments [11–14] have shown that conversion efficiencies (CEs) obtained with gas bags or gas cans filled with xenon, argon, and krypton can be higher than CE numbers obtained with solid disks. It is well known from x-ray conversion experiments and simulations that hard x-rays originate preferentially from the hot underdense region of the ablated material of the solid target. In the case of underdense gas radiator, the electron density n_e is lower than the critical density for the laser, $n_c = 1.1 \times 10^{21} / \lambda^2 = 9 \times 10^{21}$ cm^{-3}, where λ is the laser wavelength in micrometers. At n_e close to n_c, laser absorption occurs predominantly by inverse Bremsstrahlung and a large volume of plasma can be heated by a supersonically bleaching wave [11,15].

In this paper we report the conversion efficiency measurements of K-shell emission in the energy bands from 4.6 - 6.5 keV for titanium and 9 - 13 keV for germanium. Here,

multi-keV yields come from plastic hohlraums and halfraums whose inner walls have been coated by metallic material. Two series of experiments have been done on the OMEGA laser facility at the Laboratory for Laser Energetics [16,17]. A broad set of diagnostics was used to characterize the plasma such as an absolutely calibrated diode-based spectrometer, crystal spectrometers and x-ray imagers. This work follows recent x-ray-source development experiments [18-24] where the radiators were single, thin-metallic foils irradiated by two laser pulses, one of which delayed in time (materials tested were Ti, Cu and Ge).

II. OMEGA EXPERIMENTS

A. Target definition

Targets are made of plastic cylinders, also called a hohlraum or halfraum (half cylinder) into which a few-microns-thick metallic liner has been sputtered (cf figure 1). They were produced by the CEA target fabrication laboratories. They are held inside the target chamber from the target positioner in port H2. The cylinder's axis is the axis of symmetry of laser beam cones. A total of 11 targets have been used. In the first series of experiment we used six cylinders with titanium liners to test two different laser pulses shape and two target sizes. In the second series, a titanium liner has been sputtered into one halfraum and a germanium liner has been given to two cylinders and two halfraums. Atomic composition of the plastic used is: $C_{23} H_{27} O_5 N_1$, its mass composition is $C_{68.94\%} H_{6.86\%} O_{20.37\%} N_{3.37\%}$ and its density is $1.2 \pm 0.03 g\, cm^{-3}$. Liner thicknesses are 1 micron for germanium and 2 microns for titanium. Target characteristics have been gathered in

Table 1 where S-type hohlraum stands for short length and L-type for long length titanium hohlraums.

Target type	Inner diameter (mm)	Inner length (mm)	Wall thickness (mm)	Outer diameter (mm)	Outer length (mm)
Ti-L-type HOHLRAUM	1.2	3	0.4	2	3
Ti-S-type HOHLRAUM	1.6	2.5	0.1	1.8	2.5
Ti-HALFRAUM	1.6	1	0.1	1.8	1.1
Ge-HOHLRAUM	1.6	1.6	0.1	1.8	1.6
Ge-HALFRAUM	1.6	1	0.1	1.8	1.1

Table 1 Targets definition and dimensions.

B. Laser parameters

The OMEGA laser is a 60-beam facility delivering a maximum of 30 kJ at $3\omega = 351$ nm [16, 17] designed for direct drive implosions. In our experiment, a subset of the laser beams

grouped into two or three cones were focused inside the target. Different experimental parameters were investigated to get the conversion efficiency with various conditions.

In the first series of experiments the beams were equipped with polarization smoothing plates (double polarization rotator) but no other smoothing technique was used on these experiments in order to increase energy on target as it was the first test of lined cylinders as x-ray sources. All the beams pointed few millimeters outside of the target located at the chamber center in order to have optimized inner wall irradiation close to 10^{15}W/cm^2. Titanium x-ray production measurements have been done with ALPHA501P laser pulse shape for the first four shots (figure 2) to investigate the effect of plasma creation by an initial picket of laser power few nanoseconds before the main laser power. In order to maintain uniform irradiation, the three beam cones were used simultaneously, i.e., 20 beams per cylinder side for ALPHA501P. The last two shots of this series give the target yield performance with the 1ns SG1018 squared pulse shape (figure 2). The 21° cone was not used with the SG1018 pulse to avoid possible damages of OMEGA laser facility by transmitted laser power through the target.

In the second series of shots, the 42° and 59° beam cones only were used, i.e. 15 beams per irradiation side to be consistent with last two shots of first series that gave the best results. The new DPP E-IDI-300 phase plates [25] were used since they were just recently available. They give radial focal spots with a supergaussian factor of 4.1. The elliptic focal spot diameters are 106 μm and 145 μm at half maximum. Temporal smoothing (3Å) was employed as well to have plasma conditions more relevant for simulation code comparisons. This technique reduces energy from ~500 J to 445 J for the SG1018 pulse shape (figure 2).

III. DIAGNOSTICS

The five main diagnostics used in these campaigns are shown in Figure 1 relative to the target axis.

A. Laser energy measurements by FABS

FABS (Full Aperture Backscatter System) gives the absolute, time-resolved backscattered laser power of the two spectral components: Raman (weak wavelength shift relative to laser wavelength) and Brillouin (large shift). There are two FABS devices mounted on laser beams #25 and #30 that correspond respectively to the 42° and 59° beam cones. Experimental results show (Table 2) that whatever the size of the titanium hohlraum, the ALPHA501P laser pulse shape gives backscatter ratios of about 10% for 59° beam cone and about 17% for the 42° cone. An estimated backscatter ratio of 20% for the 21° beam cone gives a total absorbed energy of 87%.

With same laser smoothing parameters, the use of SG1018 pulse shape leads to a reduced backscatter and a total absorbed energy of 96%. This 10% difference can be explained for ALPHA501P pulse by the strong backscatter during the bulk of laser power at a time when the cylinder is already filled with plasma created by the first picket of laser power. IDI 300 DPPs strongly reduce backscatter to a level close to threshold detection level since the total absorbed energy is 98% for a hohlraum target (1 or 2 sided irradiation). Note that halfraums absorb all incident laser energy.

Shot number	41886	41887	41888	41889	41890	41891	46697	46698	46701	46702	46704
Target type	Ti-L type HOHLRAUM				Ti- S type HOHLRAUM	Ti-L type HOHLRAUM	Ti-HALFRAUM	Ge-HALFRAUM	Ge-HOHLRAUM		Ge-HALFRAM
Liner thickness (μm)	6	6	4	3	3	6	2	1	1	1	1
Pulse shape / number of beams	ALPHA 501P / 45 beams					SG1018 / 30 beams					
Number of sides irradiated	2 sides						1 side		2 sides	1 side	
Energie laser (J)	16630	16902	16829	17114	14532	14450	5755	5860	12897	6453	6402
Smoothing techniques	DPR and no DPP						DPP E-IDI-300 and DPR				
Ratio FABS energy with single beam energy of 42° cone	15%	17%	18%	17%	10%	6%	0%	0%	1%	1%	<1%
Ratio FABS energy with single beam energy of 59° cone	10%	9%	11%	9%	2%	3%	<1%	<1%	2%	2%	0%
Total absorbed energy with 20% (estimation) backscatter for 21°cone	87%	87%	86%	87%	96% (no 21° cone used)	96% (no 21° cone used)	99% (no 21° cone used)	99% (no 21° cone used)	98% (no 21° cone used)	98% (no 21° cone used)	99% (no 21° cone used)

Table 2 Laser energies on target and backscattered energy considerations.

A. DMX broadband spectrometer

DMX is a broadband, time-resolved spectrometer based on a x-ray diodes array [26] that measures x-ray power over a large spectral range: from 50 eV to 20 keV in its nominal configuration. For these experiments, it has been specifically setup to cover the helium-like and hydrogen-like spectral regions of titanium and germanium within the range of 4-6 keV and 9-13 keV, respectively. The spectral range of each channel was adjusted by choosing appropriate filter materials. DMX had a view at a 37.6° angle with respect to the target axis in both series of shots.

Figures 3 to 10 show temporal behavior of x-ray production measured by all the spectrally defined channels of DMX for titanium and germanium targets. These channels can be divided into 2 groups for soft x-rays measurements below 3 keV for titanium and 6 keV for germanium plasma, and above these limits for channels measuring the Ti and Ge K-shell emission. With the ALPHA501P pulse shape, Ti-L-type hohlraums give an early x-ray picket in the soft x-ray channels (figure 3) and both laser pulse shapes give an x-ray shoulder after the end of laser pulse (figures 3 and 4). This late-time phenomenon is not

5

observed in the high-energy channel measurements. The late-time soft-x-ray shoulder could be explained by plasma confinement by the target's walls after radial expansion and collision with the walls, which maintain good conditions for x-ray production longer in time. However, for the hard-x-ray signals in Figs. 3 and 4, conditions may be nevertheless too cold to give K-shell production.

This simple explanation is contradicted for hard x-rays when we compare Ti-L-type with Ti-S-type hohlraums in figures 5 and 6 and even figure 7 for the Ti-halfraum as well. With the S-type target, soft x-ray channels show a bigger shoulder slightly delayed in time that maintain x-ray production up to 4 ns rather than 3 ns for L-type and more surprisingly, hard x-ray channels have a shoulder as well. Intense K-shell emission duration (specifically measured by channels 12 and 13) is increased by 50% with Ti-S-type hohlraums and Ti-halfraum compared to Ti-L-type hohlraums. This is due to radial plasma collision on axis (see pinhole and XRFC images) that highly ionizes titanium ions and then creates a burst of K-shell emission. The radial time of flight is defined as the time for the ablated plasma to reach the cylinder axis. The radial time of flight dependence is proven as the soft x-ray shoulder appears ~1 ns later for the S-type hohlraum with its larger inner diameter than for the L-type target. For the S-type hohlraum and SG1018 laser pulse (figure 6), the hard x-ray burst appears at 1.5 ns on axis after one radius of expansion and the soft x-ray shoulder at ~3 ns which corresponds to 2 radius time of flight. This timing is more subtle with the Ti-halfraum (figure 7) because only 1/3 of total laser energy has been delivered to the target and plasma conditions are not the same. Ti-S-type hohlraum signals given by DMX are 15% more intense on all channels than L-type hohlraums but total x-ray output depends more on emission duration. Emission duration at half maximum is doubled with S-type hohlraum for the picket/main pulse shape and it is increased by 50% for 1ns squared pulse shape.

The same analysis performed on germanium x-ray yields shows the same trends (figures 8-10). A small shoulder in signals for K-shell emission (channel 15) is observed after the end of laser pulse and photons with energies below 9 keV (channels 12, 13 and 14) are also produced over a longer time scale compared to halfraum or single-sided irradiation. The soft x-ray shoulder appears now significantly earlier than for the titanium plasmas (2 ns rather than 3 ns for titanium) due to different hydrodynamic speed. This is confirmed with single-sided or two-sided irradiation of germanium hohlraums for which a soft x-ray shoulder appears clearly and at the same time (2 ns). In every case of the germanium targets employed here, no hard-x-ray shoulder produced by on axis plasma collision has been measured, probably due to an unsuitable hohlraum diameter relative to the laser energy delivered to the target. Absolute output yields will be compared to HENWAY ones in section IV.

B. HENWAY spectrometer

HENWAY [11] is a high-resolution spectrometer that gives time integrated x-ray spectra with adjustable spectral bandwidths depending on crystal and mounting choices. As this diagnostic is absolutely calibrated, it gives x-ray output in addition to DMX measurements but at a different view angle relative to the target axis. The HENWAY view angle is 60.9°. Two PET crystals have been installed with different mounting angles to look at titanium and germanium K-shell emissions. The first one gives a spectral bandwidth between 3.5 and 5.3 keV and the second crystal scatters photons of energies from 5 to 13 keV. The

detector medium is DEF film. Spectra in figure 11 show detailed structures of K-shell emission lines from titanium plasmas. The observed Helium-like resonance and intercombination He$_\alpha$ lines as well as the Ly$_\alpha$ line are strong in the upper panel. In the bottom panel, a large number of He-like and H-like titanium emission lines are intense as well. The K-shell titanium lines found in literature [27-32] are listed in table 3. These spectra give information about plasma temperature: the presence of intense hydrogen-like lines mean the plasma is highly ionized, laser absorption is good and the laser heating is efficient to produce multi-keV x-rays.

Line name	Transition levels	Photon energy (eV)
He α intercombination	$1s^2$-$1s2p\ ^3P_1$	4727
He α resonance	$1s^2$-$1s2p\ ^1P_1$	4750
Ly α intercombination	$1s$-$2p\ ^2P_{1/2}$	4966
Ly α resonance	$1s$-$2p\ ^2P_{3/2}$	4977
Li-like (satellite?)	$1s^2 2p$-$1s2p3p$	5498
Li-like (satellite?)	$1s^2 3s$-$1s2p3s$	5528
He β intercombination	$1s^2$-$1s3p\ ^1P_1$	5575
He β resonance	$1s^2$-$1s3p\ ^1P_1$	5582
Li-like (satellite?)	$1s^2 2p$-$1s2p4p$	5764
He γ	$1s^2$-$1s4p$	5873
Li-like (satellite?)	$1s^2 2p$-$1s2p5p$	5890
Ly β intercombination	$1s$-$3p\ ^2P_{1/2}$	5890
Ly β resonance	$1s$-$3p\ ^2P_{3/2}$	5893
He δ	$1s^2$-$1s5p$	6010
He ε	$1s^2$-$1s6p$	6075
He Z	$1s^2$-$1s7p$	6120
He H	$1s^2$-$1s8p$	6153
Ly γ	$1s$-$4p$	6215

Table 3 Titanium lines and respective photon energies [27-32].

Line name	Transition levels	Photon energy (eV)
He α intercombination	$1s^2$-$1s2p\ ^3P_1$	10221
He α resonance	$1s^2$-$1s2p\ ^1P_1$	10280
Ly α intercombination	$1s$-$2p\ ^2P_{1/2}$	10575
Ly α resonance	$1s$-$2p\ ^2P_{3/2}$	10624
He β intercombination	$1s^2$-$1s3p\ ^3P_1$	12081
He β resonance	$1s^2$-$1s3p\ ^1P_1$	12099
Ly β intercombination	$1s$-$3p\ ^2P_{1/2}$	12550
Ly β resonance	$1s$-$3p\ ^2P_{3/2}$	12564
Ly γ intercombination	$1s$-$4p\ ^2P_{1/2}$	13239
Ly γ resonance	$1s$-$4p\ ^2P_{3/2}$	13245
Ly ε intercombination	$1s$-$5p\ ^2P_{1/2}$	13557
Ly ε resonance	$1s$-$5p\ ^2P_{3/2}$	13560

Table 4 Germanium lines and respective photon energies [27-32].

Germanium spectra in figure 12 show strong Helium-like resonance and intercombination He_α lines, as well as the He_β lines. The absence of hydrogen-like lines is clearly observed no matter what the type of target is, showing that laser heating needs to be enhanced to get emission from this ion as well. The K-shell germanium lines found in literature [27-32] are listed in table 4. From these absolutely calibrated spectra, x-ray yields are compared with DMX ones in table 6 (cf. Discussion section).

C. Time-resolved spectrometer SSC-A

A rubidium hydrogen phthalate (RAP) crystal spectrometer has been used with a streak camera to monitor the helium- and hydrogen-like titanium lines as a function of time. Sweep speed 1 is selected to get a time-window of 5 ns. Filters used are 150 μm of beryllium and 25 μm of aluminum. The selected spectral region goes from 4 to 6 keV with the help of BIOMAX film. The view angles of this diagnostic is 37.4° relative to the P5 axis for first series and 63.4° relative to the P8 axis for second set of experiments. Time resolved spectra in figures 13 and 14 clearly show Heα, Heβ, Heγ, Lyα and Lyβ titanium lines. Around 4.5 keV, where the HENWAY spectrometer cannot give information, the K lines from neutral titanium can be seen. This occurs at beginning of the 1 ns squared pulse shape when high laser power irradiates the cold titanium. This starts K-shell atomic-level depletion and resulting x-ray emission by electrons filling these inner-shell vacancies. Normalized x-ray power traces versus time are given in figure 15 to compare the waveforms from different targets with a squared pulse shape. The S-type hohlraum gives the largest full width at half maximum, which can be related to its large inner diameter.

D. X-ray imaging by pinhole camera

The targets' x-ray emission volumes were observed by time-integrating pinhole cameras. The magnification is 4 and the total filtration was 150 μm beryllium plus 25 μm aluminum for titanium targets and 150 μm only of beryllium for germanium targets due to expected lower yield. Pinhole diameter is 11 μm. Detectors are CID (Charge Injection Device). The view angle from the hohlraum axis (toward P8 port) for the pinhole cameras is 72.2° for titanium shots and the germanium halfraum (figures 16 & 17) but 79.2° for the germanium hohlraums (figure 18). These images show well how the cavities are filled with plasmas that emit x rays above 2 keV. Most of the radiation comes from walls heated by laser spots and regions along the longitudinal axis. Emitting plasmas do not expand in the whole hohlraum volume as the emission diameter is smaller in the middle of hohlraum than near the LEH. Higher intensities observed with S-type titanium hohlraums compared to L-type ones (figure 16) can be correlated with the higher yield seen by DMX, but mainly is explained by the wall-thickness difference as L-type hohlraums have 400 μm thick plastic walls and S-type hohlraums, titanium halfraum and germanium targets have 100 μm thick walls. Emission from Ge and Ti halfraums is similar, but less intense, for the germanium target as is expected from its lower CE value. Looking carefully at the hohlraum reveals another bright spot on axis and in the middle of the cavity. This must be collision of plasmas coming from the two sides of hohlraum since this bright spot does not exist when the hohlraum is heated on one side only, nor is it seen in the halfraum images (figure 17 and 18). As a corollary, the longer duration for soft x-rays are indeed due to this radial

collision at wall (confinement effect), not an axial collision benefit. Emission from Ge and Ti halfraums are shown in figure 18, where one can see that the target behave similarly, but that the Ti emission is more intense, as expected.

E. X-ray imaging by XRFC

Time-resolved images of x-ray emission were monitored with a gated x-ray framing camera that observed the target perpendicular to its axis. The camera used a combination of pinhole array, grazing incidence mirrors, filters and a gated microchannel plate to provide temporal and spatial resolution. The time origin is the beginning of the laser pulse. Intervals between each image are 500 ps for titanium targets and 700 ps for germanium targets. These images are obtained with a 50 ps time duration. A grid of 12 pinholes is used where each pinhole is 10 μm in diameter, placed at a distance where the magnification is 2. The filters are 525 μm of beryllium to measure photons with energies greater than 3 keV.

One can easily imagine (figure 19) a ring of laser spots striking the wall of the target near the laser entrance hole at 500 ps after the laser start up. For halfraum targets and the germanium one-side irradiation case (figure 20), one emission ring only is detected, of course. Images taken at 1.4 ns and 1.5 ns show clearly that the targets are not completely filled with emitting plasma, as emission near the LEH is wider than in the middle of hohlraum. At that time, the most intense regions are no longer near the walls heated by the laser spots but rather in a region along the hohlraum axis, which is observed in all targets. Radial and axial plasma expansions make a strong plasma collision along the hohlraum axis as was clearly seen in the pinhole camera images (three bright spots along the axis). The radial dimensions of the emission decrease with time and at late time (2.1 ns image) plasma emits near the axis only.

Due to different target lengths, the axial plasma collision, which occurs after the radial plasma collision, is observed at ~1.5 ns only with the shortest hohlraum of 1.6 mm in length. With the 1.6 mm and 2.5 mm long titanium hohlraums, the axial plasma collisions cannot be seen before the end of framing camera acquisition time, but still exists as it is seen in the time-integrated pinhole camera images.

Above 3 keV emission is much weaker for germanium than titanium for similar laser irradiation as one can directly compare images from halfraums in figure 20.

For titanium, the shoulder last from 1.5 to 2 ns with SG1018 pulse shape according to DMX signals. XRFC images show that at that time (1.5 ns image), radial expansion has reached the axis but no axial collision is seen yet. So radial collision is responsible for multi-keV yields.

For germanium targets, in the 1.4 ns image we see that both radial and axial collisions are present at the time where there is a shoulder in DMX signals for channels 12-14. As single side irradiation and halfraum targets do not give the shoulder for photons between 3 to 9 keV (medium x-rays) and there is of course no axial collision, we can say that axial germanium plasma collisions make x-rays emission lasts longer.

IV. DISCUSSION ON X-RAY OUTPUT

To start discussion on multi-keV x-ray output we show in Table 5 and Table 6 x-ray energy per steradian measured in the direction of the diagnostic and resulting conversion efficiencies (CEs) assuming 4π steradian isotropic emission, to compare with other radiation sources published in literature. These data are obtained with the two absolutely

calibrated diagnostics simultaneously run on all shots, which observed the plasma emission with different view angles relative to the target axis (37.6° for DMX and 60.9° for HENWAY). CEs are defined as the ratio of measured x-ray energy within the specific spectral bandwidth divided by total laser energy. The DMX values have been assessed from unfolded spectra and by spectrally integrating over a bandwidth centered on K-shell emission lines, i.e. from 4.6 to 6.5 keV from titanium emission and from 9 to 13 keV for germanium. The overall relative uncertainty is ±20% on the CE numbers from the DMX data considering the filter transmission and detector sensitivity calibrations and the unfold treatment necessary to take into account the broadband response of the DMX channels. HENWAY data are obtained from time-integrated spectra with spectral integration over same bandwidths. Uncertainties for HENWAY CEs are ±30% resulting from crystal reflectivity measurements across the width of the crystal [11], relative transmission of differential filters and the level of film background [12].

Diagnostic	Spectral range (keV)		Ti-L-type, α501P #41886		Ti-L-type, α501P #41887		Ti-L-type, α501P #41888	
			X-ray per sr	CE in 4π	X-ray per sr	CE in 4π	X-ray per sr	CE in 4π
HENWAY	4.6	6.5	4.1×10^{-3}	5.2%	4.0×10^{-3}	5.1%	3.7×10^{-3}	4.7%
DMX	4.6	6.5	6.5×10^{-3}	8.2%	6.4×10^{-3}	8.1%	6.3×10^{-3}	7.9%

Diagnostic	Spectral range (keV)		Ti-S-type, α501P #41889		Ti-S-type, SG1018 #41890		Ti-L-type, SG1018 #41891		Ti-halfraum, SG1018 #46697	
			X-ray per sr	CE in 4π	X-ray per sr	CE in 4π	X-ray per sr	CE in 4π	X-ray per sr	CE in 4π
HENWAY	4.6	6.5	8.3×10^{-3}	10.4%	10.6×10^{-3}	13.3%	4.9×10^{-3}	6.1%	Data not available	
DMX	4.6	6.5	10.7×10^{-3}	13.4%	12.6×10^{-3}	15.8%	7.7×10^{-3}	9.7%	$11,6.10^{-3}$	14,6%

Table 5 Titanium x-ray energy normalized by laser energy per steradian measured in the direction of the diagnostic and conversion efficiency (CE) given in 4π assuming isotropic emission.

Diagnostic	Spectral range (keV)		Ge-halfraum, SG1018 #46698		Ge-hohlraum, SG1018 #46701		Ge-hohlraum, SG1018 #46702		Ti-halfraum, SG1018 #46704	
			X-ray per sr	CE in 4π	X-ray per sr	CE in 4π	X-ray per sr	CE in 4π	X-ray per sr	CE in 4π
HENWAY	9	13	7.3×10^{-4}	0.9%	8.4×10^{-4}	1.0%	8.0×10^{-4}	1.0%	5.9×10^{-4}	0.7%
DMX	9	13	4.6×10^{-4}	0.6%	6.4×10^{-4}	0.8%	4.3×10^{-4}	0.5%	5.0×10^{-4}	0.6%

Table 6 Germanium x-ray energy normalized by laser energy per steradian measured in the direction of the diagnostic and conversion efficiency (CE) given in 4π assuming isotropic emission.

Significant differences can be seen between DMX and HENWAY yields for titanium emission. CEs shown here are calculated with the assumption of an isotropic emission lobe. This is true for germanium radiation above 10 keV but not for titanium from 4.7 to 6 keV where the relatively thick target walls absorb a significant part of the photons. The target walls are made of plastic whose formula is C_{23}-H_{27}-O_5-N_1. Transmission values through 100 μm and 400 μm thicknesses of this plastic are 70% and 25% only [33]. Furthermore,

we have to consider the real absorption length of photons passing through the wall that are specifically seen by DMX and HENWAY (wall thickness / sin[diagnostic view angle]). For the titanium L-type hohlraum, transmission of the most intense line, He_α at 4.7 keV, through 656 µm is 10% as DMX sees and 20% as HENWAY sees the target. For other targets, transmission of the same titanium line is 57% for DMX and 67% for HENWAY.

Considering that the walls are relatively opaque for titanium radiation, measurement discrepancies between HENWAY and DMX can be explained by the apparent LEH surface area for the L-type hohlraum, since most of radiation comes from the LEH due to the thick walls. The DMX values are higher by a factor of 1.6 because the ratio between apparent LEH surfaces is also different by a factor of 1.6. For the S-type hohlraums, photon contributions come mainly from the LEH but also from x rays passing through the target wall. Energies measured by the 2 diagnostics vary by factor 1.3, which means that HENWAY sees photons emitted in the whole volume of the target and passing the walls.

Transmission of the germanium He_α line at 10.3 keV is 95% through the longest apparent length (164 µm) in the target wall, meaning radiation is nearly isotropic. For germanium only, HENWAY gives higher values than DMX and the argument of LEH apparent size is not valid anymore.

The CE of the titanium halfraum is similar to the two-sided irradiation cases for the Ti-lined hohlraums. For germanium, the halfraums give lower efficiencies, probably because an absorbed-laser-energy threshold has not been exceeded to heat and ionize the germanium plasma strongly enough to emit the K-shell lines. One can note that the halfraum gives about same yield as the hohlraum irradiated on a single side. This feature removes a constraint to use these targets as backlighter since one could shoot the target from one side and use the x-rays coming out the other side.

V. CONCLUSION

Hohlraums and halfraums with inner walls coated with metallic materials have been tested for the first time as multi-keV x-ray sources. These experiments used two laser pulse shapes, with and without phase plates, and, in addition, a variety of target dimensions. Best yields have been obtained with a 1 ns squared pulse with phase plates optimized for indirect drive, which resulted in laser absorption in the target near 99%. For titanium, conversion efficiencies are up to ~14% into 4π integrating between 4.5 and 6.5 keV, when a large-inner-diameter hohlraum is used. Germanium CE is ~0.9% into 4π between 9 and 13 keV. These high CEs are due to two phenomena: long-lasting, favorable plasma conditions for multi-keV x-ray production that are maintained by plasma confinement inside the plastic cylinder, and also by radial, in addition to axial, plasma collisions, leading to bursts of x rays at a time that depends on target size. The CEs from these hohlraums are compared to those obtained with thick foils [3,5,7,8], thin pre-exploded foils [19-21], gas targets [11,12] and aerogels [13]. Figure 21 is a summary of published CEs for nanosecond laser-produced plasmas and a large variety of target materials. As titanium emitters at 4.7 keV, hohlraums are the most efficient solid targets and these data are close to gas targets, which are considered as an upper limit for x-ray yields since their low density allows good laser absorption and small kinetic losses. Titanium-hohlraum CEs are higher than those from exploded foils, thick targets and aerogels, respectively. For higher photon energies this order is changed and for copper emitters at 8 keV, exploded foils, thick targets and aerogels

give approximately the same output. Beyond this, at 10.3 keV for germanium emitters, exploded foils give the best results, one order of magnitude more efficient than thick targets. Aerogels and hohlraums give similar yields, about ~3 times lower than those of exploded foils. The very good performances of hohlraums at 4.7 keV are not confirmed at 10.3 keV. Germanium hohlraum CEs likely can be increased by creating higher temperatures in the target plasma, generating a more favorable ionization balance for emission from He-like and H-like lines, as well as by scaling the target diameter and length more appropriately to the laser energy input.

1 O. L. Landen, D. R. Farley, S. G. Glendining et al., Rev. Sci. Instrum. 72, 627 2001.
2 A. B. Bullock, O. L. Landen, and D. K. Bradley, Rev. Sci. Instrum. 72, 686 2001.
3 J. Workman, J. R. Fincke, P. Keiter et al., Rev. Sci. Instrum. 75, 3915 2004.
4 B. Yaakobi, P. Bourke, Y. Conturie et al., Opt. Commun. 38, 196 1981.
5 D. Matthews, E. M. Campbell, N. M. Ceglio et al., J. Appl. Phys. 54, 4260 1983.
6 D. W. Phillion and C. Hailey, Phys. Rev. A 34, 4886 1986.
7 J. Workman and G. Kyrala, Proc. SPIE 4504, 168 2001.
8 R. L. Kauffman in Handbook of Plasma Physics, edited by A. M. Rubenchik and S. Witkowski Elsevier Science, North-Holland, 1991, Vol. 3, pp. 111–162.
9 D. Riley, N. C. Woolsey, D. McSherry et al., Plasma Sources Sci. Technol. 11, 484 2002.
10 J. Koch, K. G. Estabrook, J. D. Bauer et al., Phys. Plasmas 2, 3820 1995.
11 C. A. Back, J. Grun, C. Decker et al., Phys. Rev. Lett. 87, 275003 2001.
12 C. A. Back, J. Davis, J. Grun et al., Phys. Plasmas 10, 2047 2003.
13 K. B. Fournier, C. Constantin, J. Poco et al., Phys. Rev. Lett. 92, 165005 2004.
14 K. B. Fournier, C. Constantin, J. Poco et al., Proc. SPIE 5196, 194 2004.
15 J. Denavit and D. W. Phillion, Phys. Plasmas 1, 1971 1994.
16 J. M. Soures, R. L. McCrory, C. P. Verdon et al., Phys. Plasmas 3, 2108 1996.
17 T. R. Boelhy, D. L. Brown, R. S. Craxton et al., Opt. Commun. 133, 495 1997.
18 M. Primout, J. X-Ray Sci. Technol. 13, 23 2005.
19 F. Girard, J.P. Jadaud, M. Naudy, B. Villette D. Babonneau, M. Primout, M. C. Miller, R. L. Kauffman, L. J. Suter, J. Grun, JF Davis**,** Phys. Plasmas, 12, 092705 2005
20 F. Girard, JP. Jadaud, M. Naudy et al., Proc. SPIE 5196, 220 2004.
21 D. Babonneau, M. Primout, F. Girard et al., Phys. Plasmas,15, 092702, 2008.
22 M. Primout et al., Journal of Physics: conference series 112 (2008) 042051
23 M. Tanabe et al., App. Phys. Letters, 93, 051505 (2008)
24 M. Tanabe et al., Journal of Physics: conference series 112 (2008) 022076
25 S. Regan ref pour E-IDI-300 DPP……………….
26 JL. Bourgade, B. Villette, JL. Bocher et al., Rev. Sci. Instrum. 72, 1173 2001.
27 R. E. Marrs, S. R. Elliott, and Th. Stöhlker, Phys. Rev. A 52, 3577–3585 1995
28 J. Sugar and A. Musgrove, J. Phys. Chem. Ref. Data 22(5), 1213–1278 1993
29 S. MacLaren, P. Beiersdorfer, D. A. Vogel, D. Knapp, R. E. Marrs, K. Wong, and R. Zasadzinski, Phys. Rev. A 45, 329–332 1992

30 Y. Funatake, T. Shirai, and Y. Nakai, Japan Atomic Energy Research Institute Report JAERI-M 87-053, 140 pp. Tokai-mura, Japan, 1987

31 J. Sugar and C. Corliss, J. Phys. Chem. Ref. Data 14, Supplement No. 2 1985.

32 M. Bitter, S. von Goeler, S. Cohen, K. W. Hill, S. Sesnic, F. Tenney, J. Timberlake, U. I. Safronova, L. A. Vainshtein, J. Dubau, M. Loulergue, F. Bely-Dubau, and L. Steenman-Clark, Phys. Rev. A 29(2), 661–674 1984

33 B.L. Henke, E.M. Gullikson, and J.C. Davis. X-ray interactions: photoabsorption, scattering, transmission, and reflection at E=50-30000 eV, Z=1-92, Atomic Data and Nuclear Data Tables Vol. 54 (no.2), 181-342 1993

Figure 1 Targets are cylinder or halfraum made of plastic with titanium or germanium liner on inner walls.

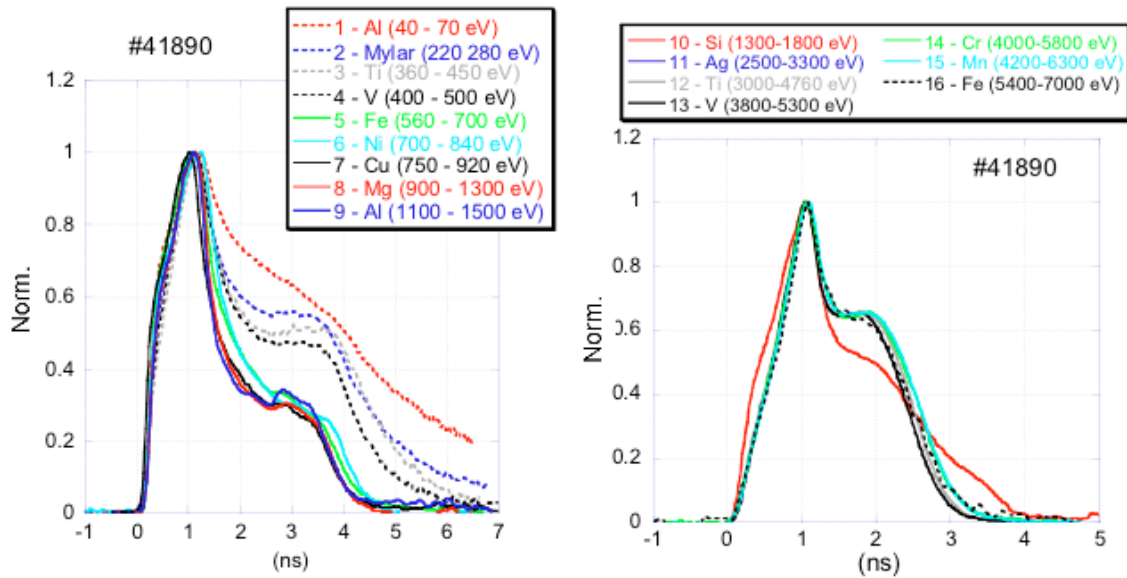**Figure 2 Laser power versus time for ALPHA501P (left) and SG1018 pulse shapes.**
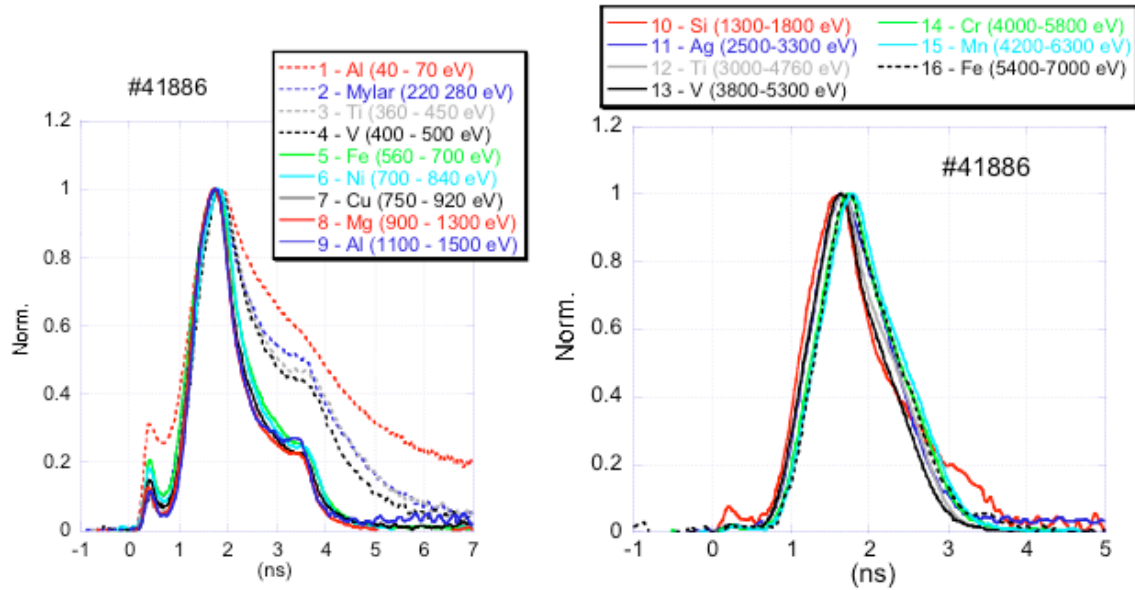
Figure 3 Normalized x-ray power versus time from DMX for the type Ti-L type HOHLRAUM target irradiated by both sides with the ALPHA501P pulse shape (shot #41886). Low energy channels are on the left hand side and high energy channels measuring the K-shell emissions are shown on the right.
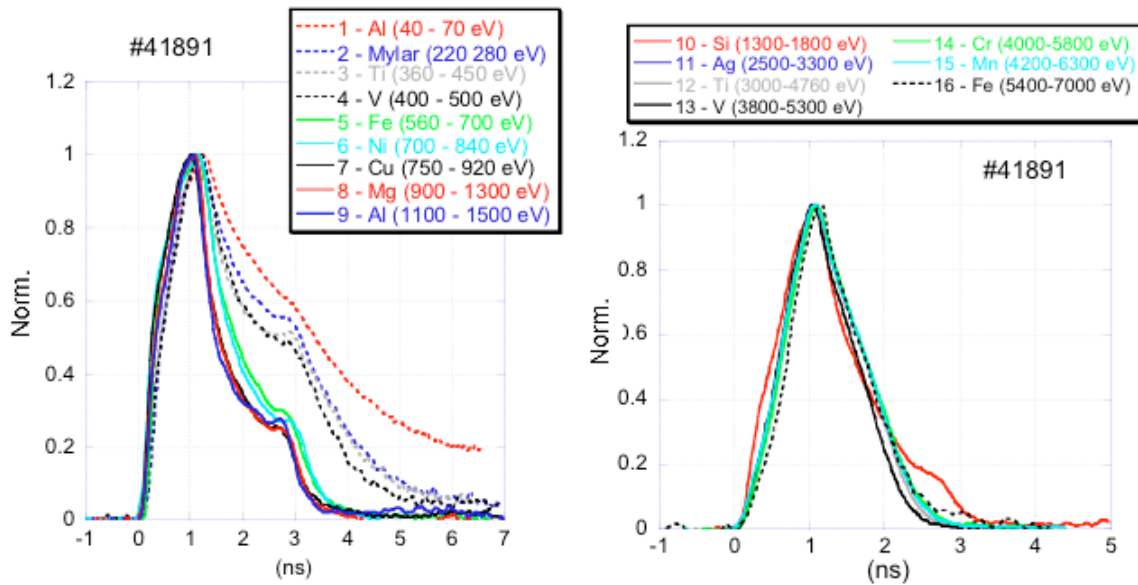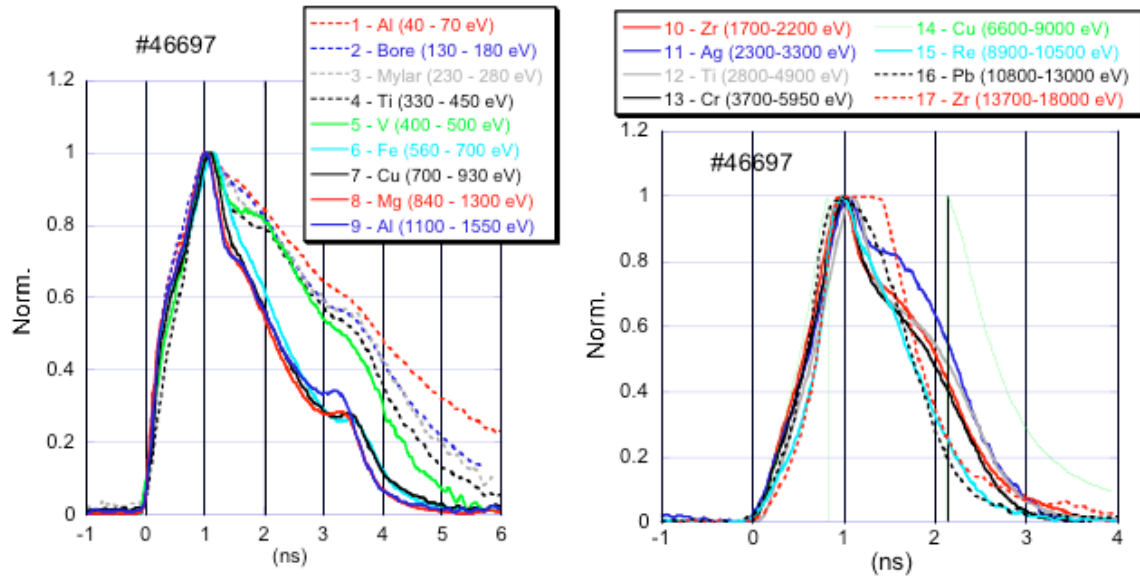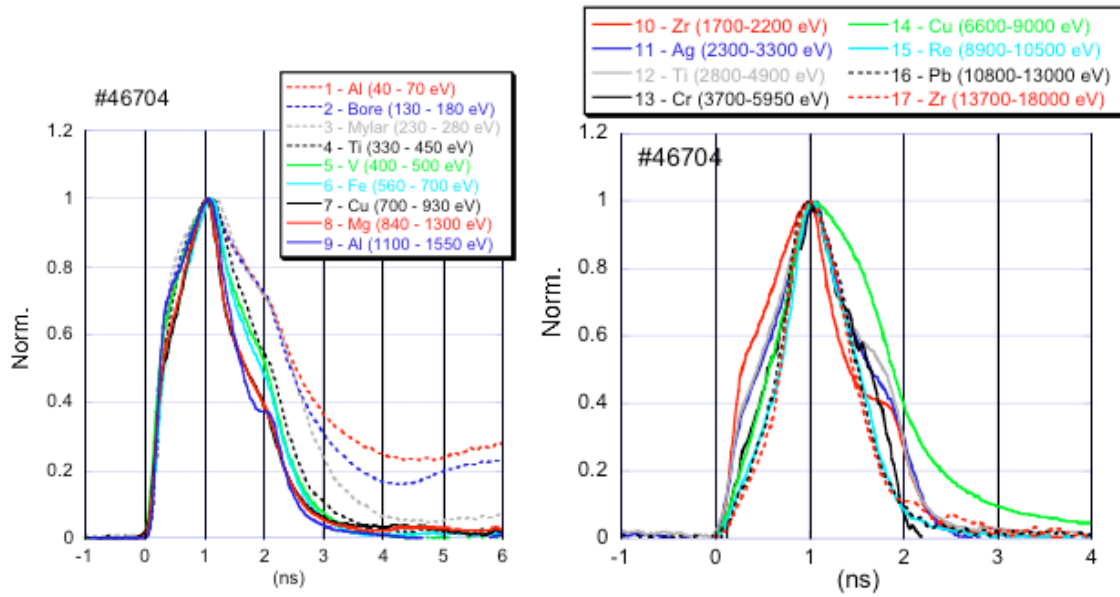

Figure 4 Normalized x-ray power versus time from DMX for the type Ti-L type HOHLRAUM target irradiated by both sides with the SG1018 pulse shape (shot #41891). Low energy channels are on the left hand side and high energy channels measuring the K-shell emissions are shown on the right.
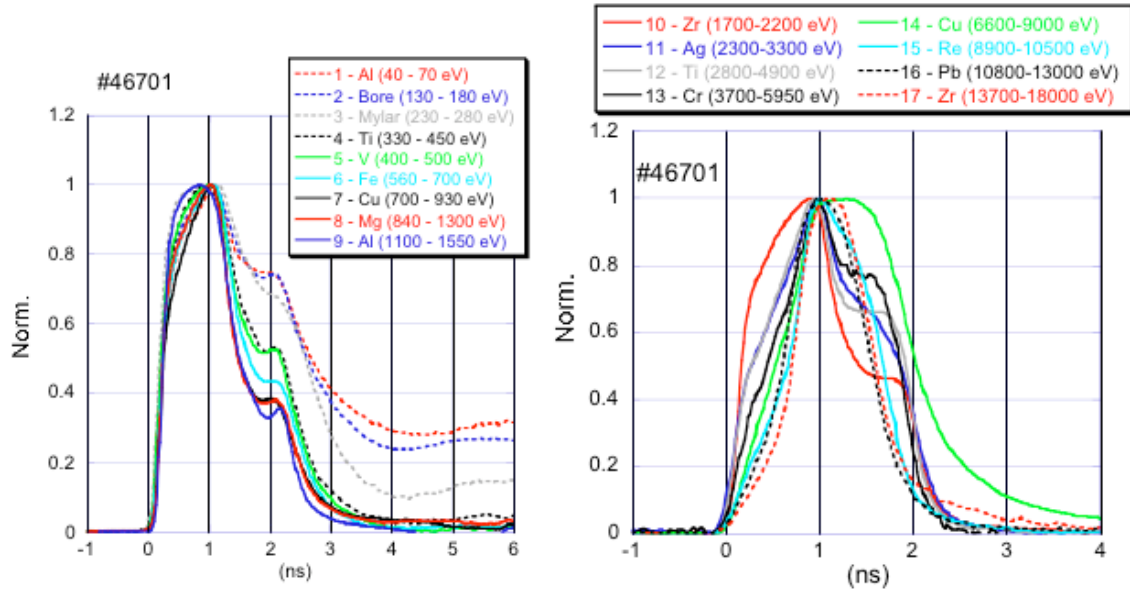
4
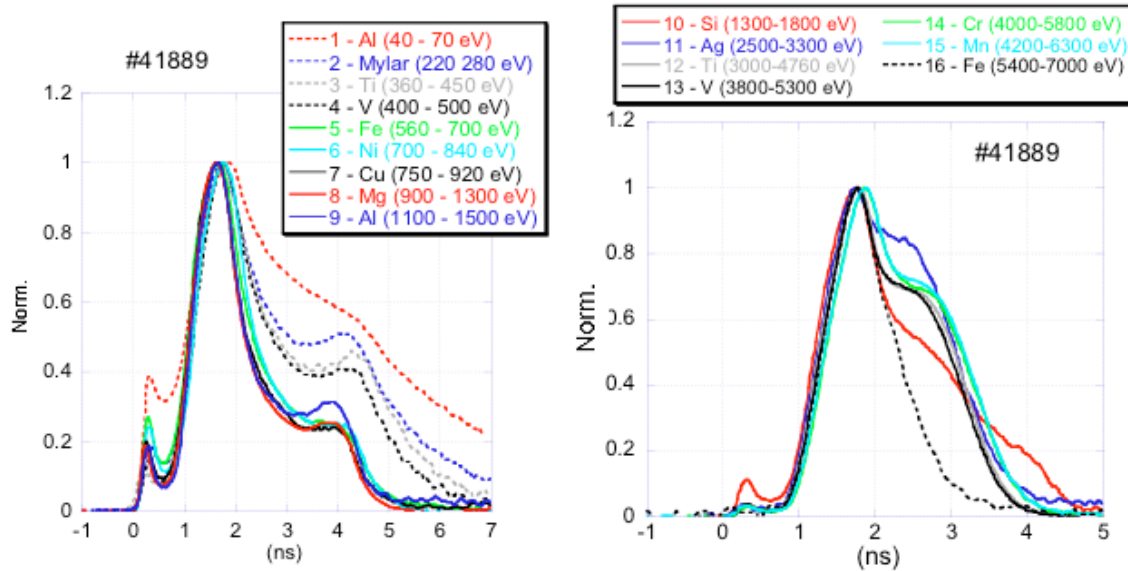
Figure 5 Normalized x-ray power versus time from DMX for the type Ti-S type HOHLRAUM target irradiated by both sides with the ALPHA501P pulse shape (shot #41889). Low energy channels are on the left hand side and high energy channels measuring the K-shell emissions are shown on the right
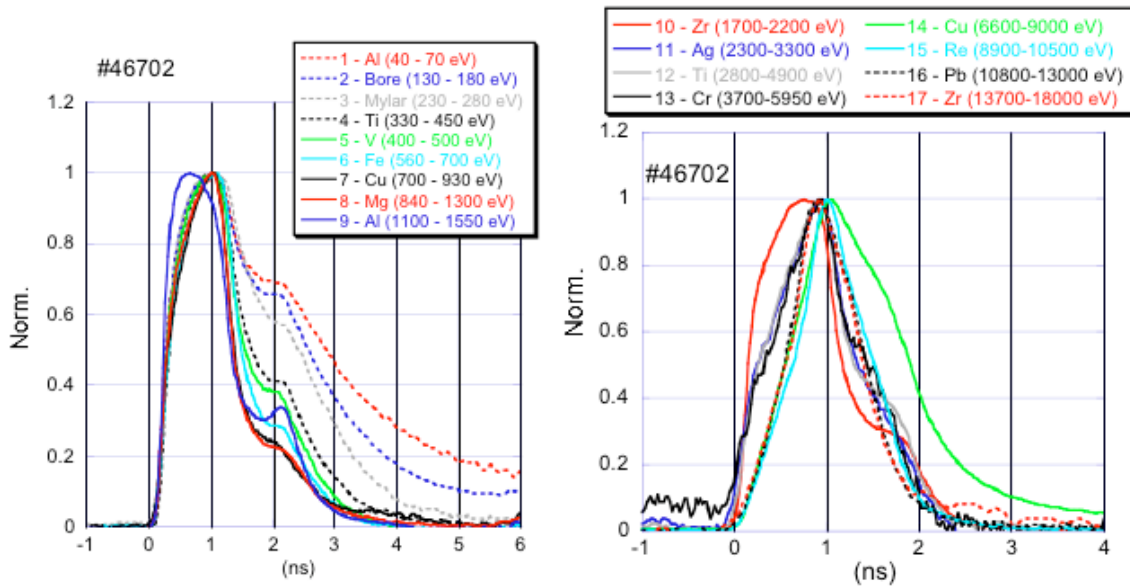

Figure 6 Normalized x-ray power versus time from DMX for the type Ti-S type HOHLRAUM target irradiated by both sides with the SG1018 pulse shape (shot #41890). Low energy channels are on the left hand side and high energy channels measuring the K-shell emissions are shown on the right.

Figure 7 Normalized x-ray power versus time from DMX for the type Ti-HALFRAUM target irradiated by one side (P8 port side) with the SG1018 pulse shape (shot #46697). Low energy channels are on the left hand side and high energy channel measuring the K-shell emissions are shown on the right. Channels 14 and 17 are saturated.


Figure 8 Normalized x-ray power versus time from DMX for the type Ge-HALFRAUM target irradiated by one side (P8 port side) with the SG1018 pulse shape (shot #46704). Low energy channels are on the left hand side and high energy channels measuring the K-shell emissions are shown on the right.

Figure 9 Normalized x-ray power versus time from DMX for the type Ge-HOHLRAUM target irradiated by two sides with the SG1018 pulse shape (shot #46701). Low energy channels are on the left hand side and high energy channels measuring the K-shell emissions are shown on the right.

Figure 10 Normalized x-ray power versus time from DMX for the type Ge-HOHLRAUM target irradiated by one side (P5 port side) with the SG1018 pulse shape (shot #46702). Low energy channels are on the left hand side and high energy channels measuring the K-shell emissions are shown on the right
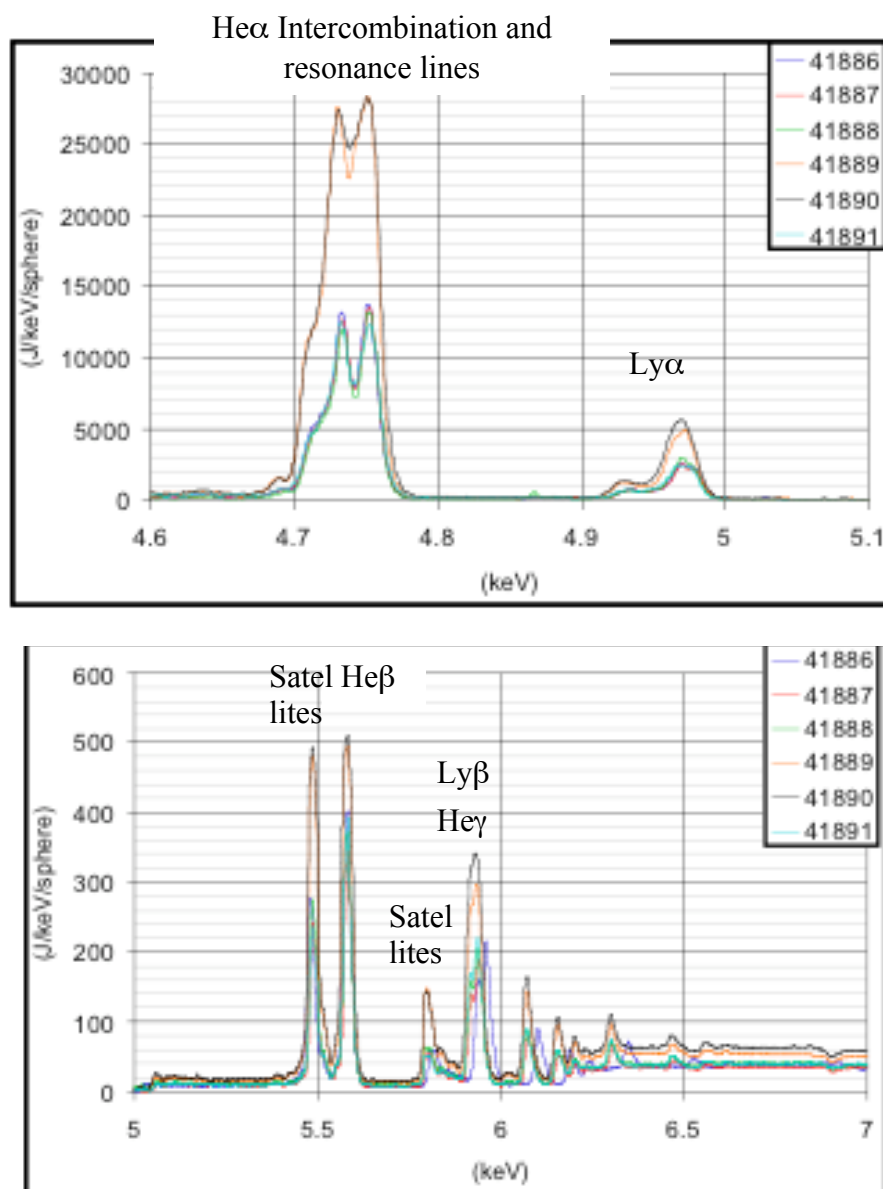
Figure 11 Titanium detailed spectra of K-shell emission lines from HENWAY for the first series of shots by using two crystal settings.
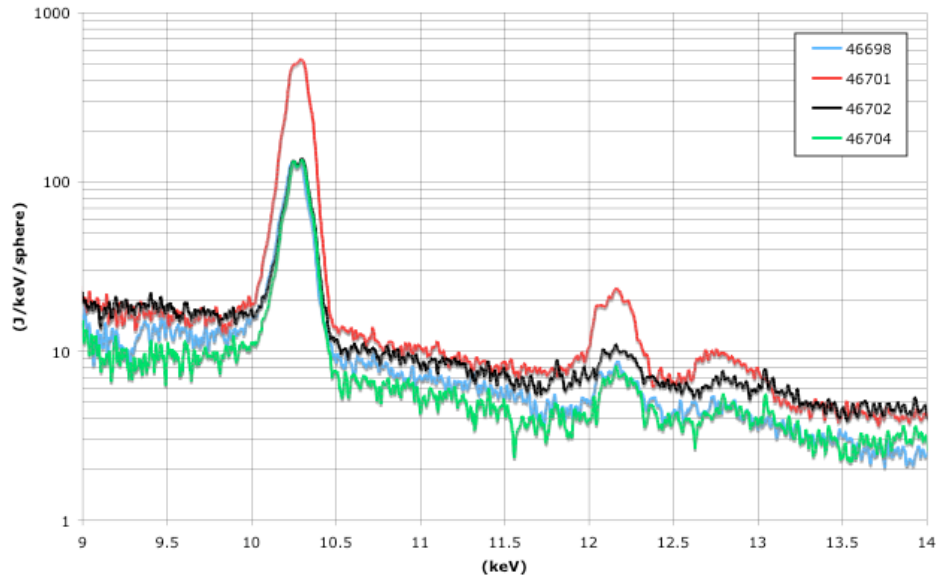
Figure 12 Germanium detailed spectra obtained from HENWAY for the second series of shots.
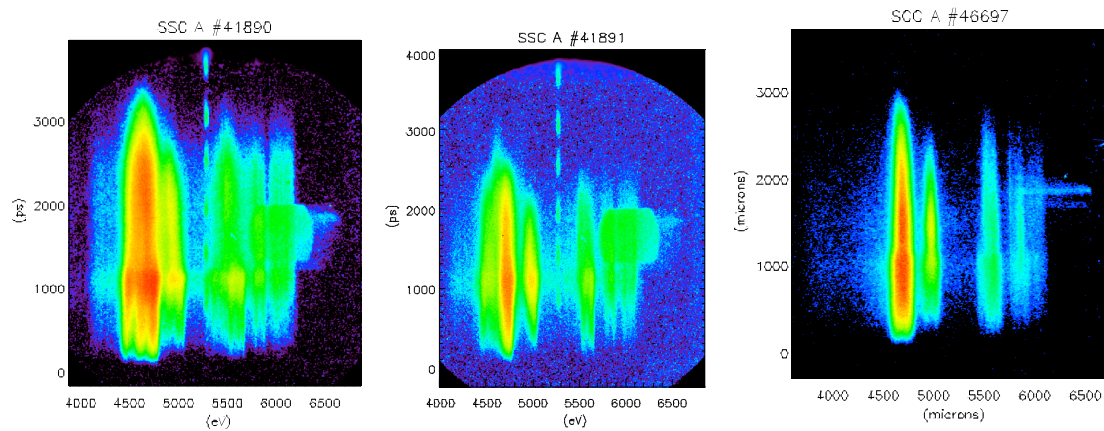
Figure 13 SSC-A streak camera images show titanium emission between 4 and 6 keV versus time for comparison between S type hohlraum (left), L type hohlraum (middle) and halfraum (right).
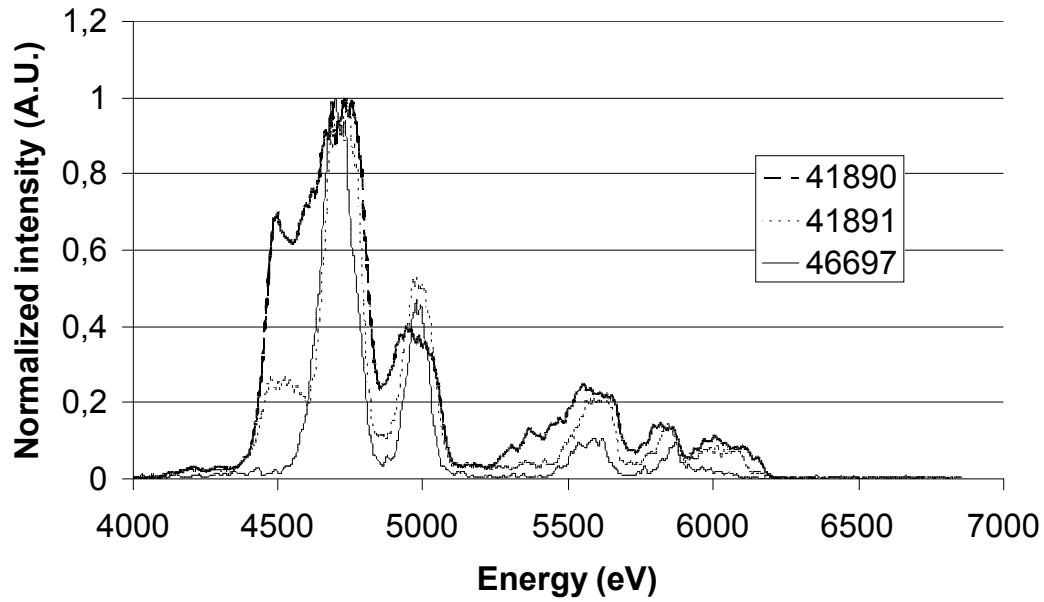
Figure 14 Spectral lineouts from SCC-A streak cameras images to compare emission spectra at the time of maximum x-ray production for L-type hohlraum (#41891), S-type hohlraum (#41890) and halfraum 1 side irradiation toward P8 (#46697) with SG1018 laser pulse shape.
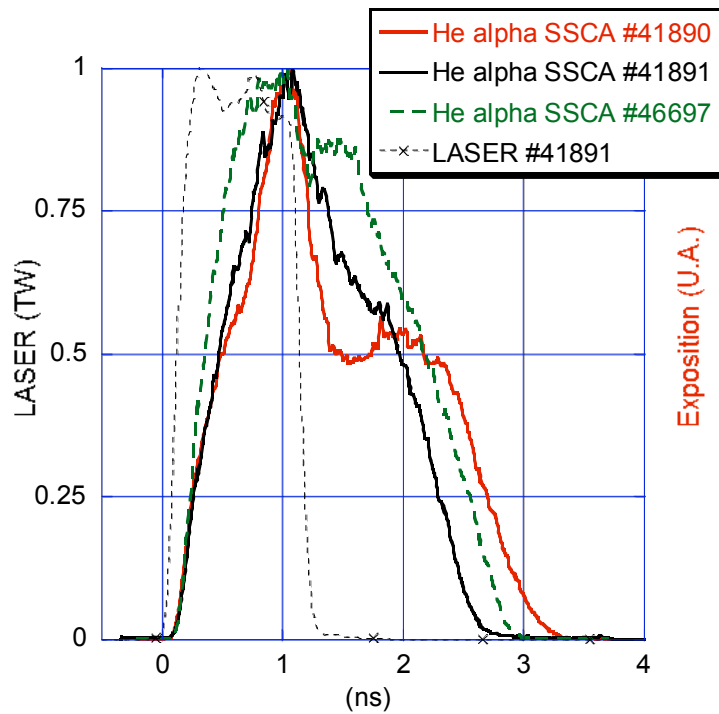
Figure 15 Temporal lineouts from SCC-A streak cameras images to compare x-ray power of titanium He$_a$ line from L-type hohlraum (#41891), S-type hohlraum (#41890) and halfraum 1 side irradiation toward P8 (#46697). (3 courbes + laser(t) sur un meme graph)
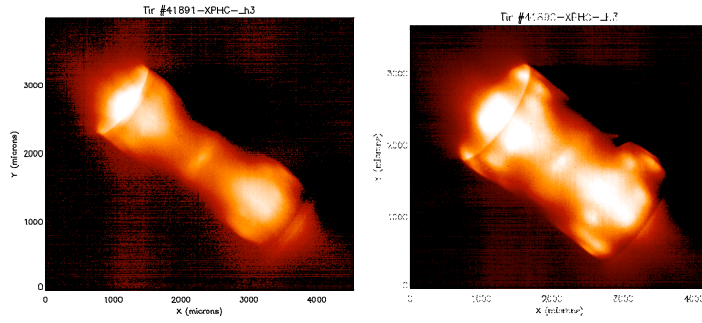
Figure 16 Pinhole camera images show titanium emission obtained with SG1018 pulse shape from L-type hohlraum (#41891 left), S-type hohlraum (#41890 right).
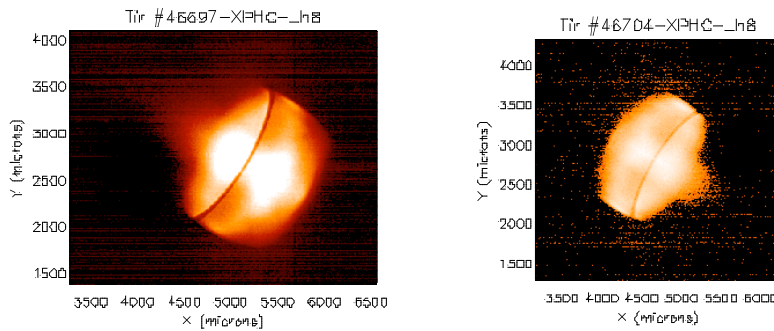

Figure 17 Pinhole camera images show halfraums emission with single side irradiation toward P8 for titanium (#46697 left) and germanium (#46704 right image).
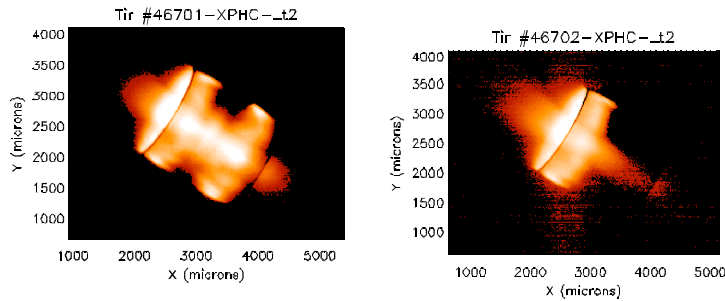

Figure 18 Pinhole camera images show germanium emission from hohlraum two sides irradiation (#46701 left) and hohlraum single side irradiation toward P5 (#46702 middle).
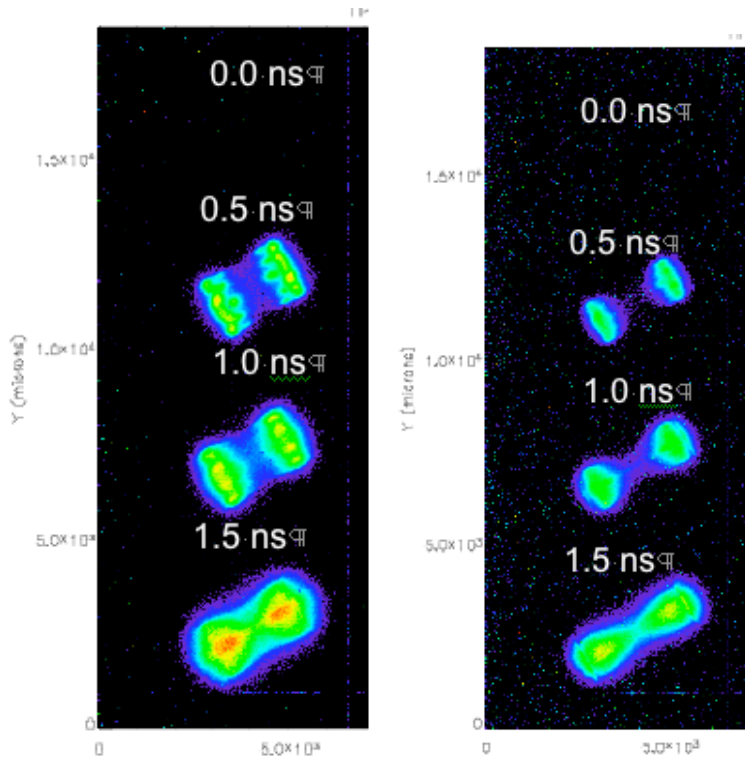
Figure 19 X-ray framing camera images showing titanium emission versus time with 1ns squared pulse shape for S-type holraum (#41890 left), L-type hohlraum (#41890 right image).
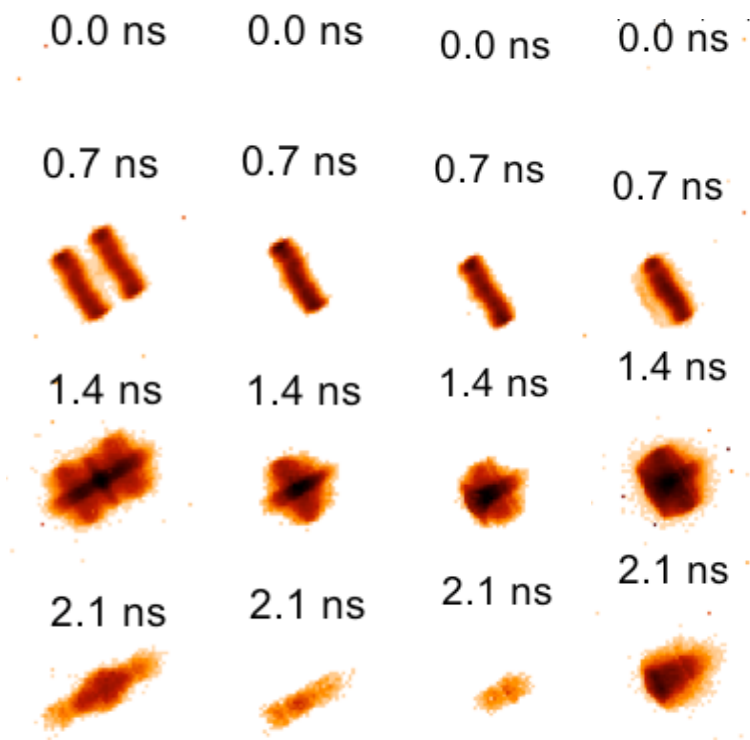
Figure 20 X-ray framing camera images showing germanium emission versus time with 1ns squared pulse shape from hohlraum 2 sides irradiation (#46701 left), hohlraum 1 side irradiation toward P5 (#46702 the 2nd image from left) and halfraum 1 side irradiation toward P8 (#46704 the 3rd image from left) and Titanium halfraum (#46697 right image)
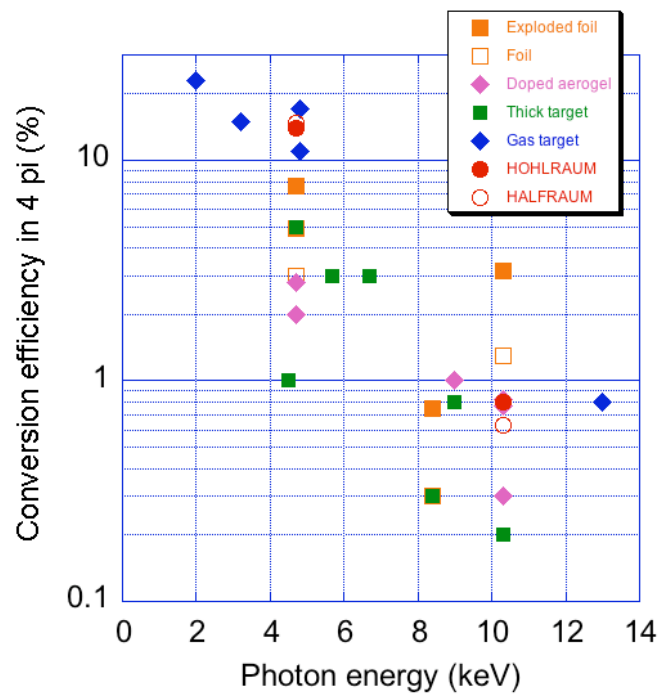
Figure 21 Summary of multi-keV conversion efficiencies for a large variety of target kinds and emitting materials.